Frontiers of Physics
https://doi.org/10.1007/s11467-018-0869-9
Front. Phys.
14(2), 23501 (2019)

LETTER

Enhanced robustness of zero-line modes in graphene via magnetic field

Ke Wang[1,2], **Tao Hou**[1,2], **Yafei Ren**[1,2], **Zhenhua Qiao**[1,2,†]

[1] *ICQD, Hefei National Laboratory for Physical Sciences at Microscale, and Synergetic Innovation Centre of Quantum Information and Quantum Physics, University of Science and Technology of China, Hefei 230026, China*
[2] *CAS Key Laboratory of Strongly-Coupled Quantum Matter Physics and Department of Physics, University of Science and Technology of China, Hefei 230026, China*
Corresponding author. E-mail: [†] *qiao@ustc.edu.cn*
Received October 20, 2018; accepted October 24, 2018

We systematically studied the influence of magnetic field on zero-line modes (ZLMs) in graphene and demonstrated the physical origin of their enhanced robustness by employing nonequilibrium Green's functions and the Landauer–Büttiker formula. We found that a perpendicular magnetic field can separate the wavefunctions of the counter-propagating kink states into opposite directions. Specifically, the separation vanishes at the charge neutrality point and increases as the Fermi level deviates from the charge neutrality point and can reach a magnitude comparable to the wavefunction spread at a moderate field strength. Such spatial separation of oppositely propagating ZLMs effectively suppresses backscattering and is more significant under zigzag boundary condition than under armchair boundary condition. Moreover, the presence of magnetic field enlarges the bulk gap and suppresses the bound states, thereby further reducing the scattering. These mechanisms effectively increase the mean free paths of the ZLMs to approximately 1 μm in the presence of a disorder.

Keywords graphene, topological state, zero-line state, electronic transport

Recently, topologically nontrivial phases have attracted much attention because of their theoretical novelty and the potential applications in dissipationless electronics of their robust edge states, which are topologically protected from backscattering [1–6]. For the quantum Hall effect and the quantum anomalous Hall effect, the edge states are chiral with oppositely propagating edge states distributed at two boundaries of the sample. The spatial separation of counter-propagating states strongly suppresses backscattering against any type of impurity [7–10]. For the quantum spin Hall effect, the edge states are spin-helical and only robust against elastic backscattering from nonmagnetic impurities because of the topological protection by the time-reversal invariance [11]. Although these edge states are robust, their presence requires a flawless boundary and manipulating them experimentally is difficult. Although these edge states are robust and have been realized in experiments, their practical application is difficult because of the requirement of strong magnetic field for quantum Hall effect or the introduction of both spin-orbit coupling and ferromagnetism for quantum anomalous Hall effect.

Different from the above symmetry-protected edge states, for the quantum valley Hall effect, although there is no rigorous bulk-edge correspondence, zero-line modes (ZLMs), also known as kink states, appear along the interface between regions with different valley topologies [3]. These helical ZLMs are protected by their large momentum separation, and short-range disorders can induce backscattering. However, because of the large wavefunction expansion, these modes are still quite robust against disorders and exhibit zero bending resistance [12]. More importantly, these one-dimensional ZLMs are highly tunable. By applying spatially varying electric field to a chiral stacking bilayer graphene (BLG) system, one can construct a single zero line, crossing double zero lines, and even zero line networks, exhibiting promising potential for applications in low-energy-consumption electronics [13–15]. Recently, a single zero and crossing double zero lines have been realized experimentally in BLG systems through careful gate alignment [16, 17] and in samples with stacking line defects [16, 18].

Inspired by the experimental results that suggest strong enhancement of the robustness of ZLMs by magnetic field, herein, we investigate the transport properties of ZLMs in gated BLG systems under perpendicular magnetic field to reveal the underlying physical origin. By varying the strength of the magnetic field, we systematically study the evolution of the electronic structure and the ZLMs wavefunctions. We find that the presence of magnetic field enlarges the bulk band gap and preserves the ZLMs. However, the wavefunctions of counter- propagating ZLMs en-

coding with different valleys are pushed apart. The spatial separation increases with the magnetic-field strength. Moreover, at a given magnetic- field strength, spatial separation exhibits strong dependence on the Fermi energy. By decreasing the Fermi level from above the charge neutrality point, spatial separation decreases, vanishes at the charge neutrality point, and then increases again while in opposite direction as the Fermi level is decreased further. The spatial separation of counter-propagating wavefunctions strongly suppresses backscattering and makes the ZLMs more robust, as confirmed by our numerical calculations of conductances in the presence of a disorder. These results suggest that the presence of magnetic field not only increases the robustness of ZLMs but also makes it possible to tune the transport by varying the Fermi level electrically.

The quantum valley Hall effect can be realized in AB-stacked bilayer graphene by applying perpendicular electric field. When opposite electric fields are applied in neighboring regions, as illustrated in Fig. 1(a), where downward (upward) electric field is applied in the region on the left (right), as denoted by the blue arrows. In the presence of an Anderson-type disorder, the π-orbital tight-binding Hamiltonian of this system can be expressed as

$$H = -t\sum_{\langle i,j\rangle}(c_i^\dagger c_j + \text{H.c.}) - t_\perp \sum_{\langle i\in T, j\in B\rangle}(c_i^\dagger c_j + \text{H.c.}) + \sum_{i\in T} U_i c_i^\dagger c_i - \sum_{i\in B} U_i c_i^\dagger c_i + \sum_i \epsilon_i c_i^\dagger c_i, \quad (1)$$

where $c_i^\dagger$ (c_i) is the electron creation (annihilation) operator on site i. The first and second terms represent the intralayer and interlayer nearest-neighbor hopping, respectively, with hopping amplitudes of $t = 2.6$ eV and $t_\perp = 0.34$ eV. The third and fourth terms indicate the site energies at the top and bottom layers, respectively. In the part on the left (right), the on-site energy U_i is constant at $+U$ ($-U$). In the interface region of width w, we use a cosinusoidal potential profile to connect the on-site energies of the two sides. The last term represents the on-site Anderson disorder, with ϵ_i being distributed randomly in the energy interval of $[-W/2, W/2]$, where W measures the disorder strength. In our calculations, we set the system width to $d = 127.8$ nm and the interface region width to $w = 85.2$ nm for both boundary condition. Note that we neglect the spin degree of freedom because the QVHE only involves the orbital degree of freedom of an electron.

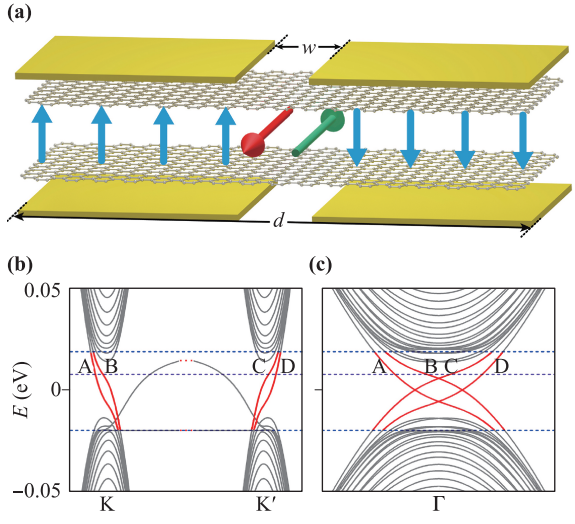

Fig. 1 **(a)** Schematic of a dual-split-gated bilayer graphene (BLG) device. The blue arrows show the direction of the electric field. The green and red arrows correspond to modes that carry valley indexes K and K′, respectively. **(b, c)** Electronic structure of the junction in the device shown in (a) with zigzag boundary (b) and with armchair boundary (c); the voltages in the adjoining regions are the opposite.

In the presence of a perpendicular magnetic field $\boldsymbol{B} = \nabla \times \boldsymbol{A}$, the tight-binding Hamiltonian model is modified by introducing the Peierls phase in the hopping terms as follows:

$$t_{ij} \to t_{ij} \mathrm{e}^{-\mathrm{i}\frac{e}{\hbar}\int \boldsymbol{A}\cdot \mathrm{d}\boldsymbol{l}}, \quad (2)$$

where $\int \boldsymbol{A}\cdot \mathrm{d}\boldsymbol{l}$ is the integral of the vector potential from site j to site i. In our calculations, we adopt the Landau gauge of $\boldsymbol{A} = -By\boldsymbol{e}_x$ for the perpendicular magnetic field $\boldsymbol{B} = B\boldsymbol{e}_z$. This gauge preserves the translation symmetry in the x direction, meaning that we can still study the electronic structure along the ZL direction.

With this π-band tight-binding Hamiltonian, we further study the ZLM transport properties using a two-terminal Landauer–Büttiker formalism based on the Green's function technique [19]

$$G_{\mathrm{RL}} = \frac{2e^2}{h}\mathrm{Tr}[\Gamma_{\mathrm{R}} G^r \Gamma_{\mathrm{L}} G^a], \quad (3)$$

where $G^{r(a)}$ is the retarded (advanced) Green's function of the central scattering region. $\Gamma_{\mathrm{R(L)}} \equiv \mathrm{i}[\Sigma^r_{\mathrm{R(L)}} - \Sigma^a_{\mathrm{R(L)}}]$ is the line width function, which describes the coupling between the right (left) lead and the central scattering region. $\Sigma^{r(a)}$ is the retarded (advanced) self-energy of the half-infinite leads calculated using the variant transfer matrix method [20]. In our calculations, we set the Fermi level to be in the band gap. In the presence of a disorder, each data point is obtained by averaging the results of 30 samples with different disorder configurations.

In the absence of a disorder, the system exhibits translation symmetry along the zero line direction, allowing us to obtain the electronic structure of the system by directly diagonalizing the tight-binding Hamiltonian. When the applied electric fields in the left and right regions are opposite to each other [as shown in Fig. 1(a)], counter-propagating topological ZLMs appear in the interface region of width w (as indicated by the red and green arrows). With a layer potential difference of $2U = 0.04$ eV, we calculate the band structure in the absence of a magnetic

field. The results are shown in Figs. 1(b) and (c) wherein gapless ZLMs (marked in green) appear in valleys K and K′ for ribbon with zigzag boundary and Γ point for ribbon with armchair boundary. Apart from the ZLMs, there are also some edge states (marked in gray) inside the band gap for zigzag boundary condition, which are localized at the sample boundaries. In contrast, when the electric fields in the left and right sides point in the same direction, the gapless ZLMs disappear.

In the following discussion, we focus on the case of opposite electric fields in the two sides of the interface. For both zigzag boundary and armchair boundary condition, there are four ZLMs inside the band gap (as denoted by A, B, C, and D in Figs. 1(b) and (c) with Fermi energy $E_F = 0.004$ eV. Figure 2(a) shows a magnified view of the band structure in valley K of junction with zigzag boundary. The wavefunctions of A and D, which are located in valleys K and K′, respectively, are shown in Fig. 2(e), where we find that the wavefunctions from both valleys coincide with each other. In the presence of a magnetic field, the band structure is modified as shown in Figs. 2(b)–(d). From these figures, we find that the presence of a magnetic field enhances the bulk band gap and lifts the bulk bands away from the ZLMs plotted in red. As the band gap increases, the ZLM wavefunctions narrow, as shown in Figs. 2(f)–(h). Moreover, we find that the presence of magnetic field drives the ZLM wavefunction in valley K upward and that in valley K′ downward, thereby reducing the overlap between counter-propagating states. The situation for armchair boundary condition is similar to zigzag edge. Figure 3(a) shows a magnified view of the band structure in Γ point. The variation of wavefunctions of A and D located near Γ point as shown in Figs. 3(e)–(h). We can see that the magnetic field have the same effect for both zigzag and armchair edges, but the spatial separation of oppositely propagating ZLMs is more significant in zigzag boundary condition than in armchair boundary condition.

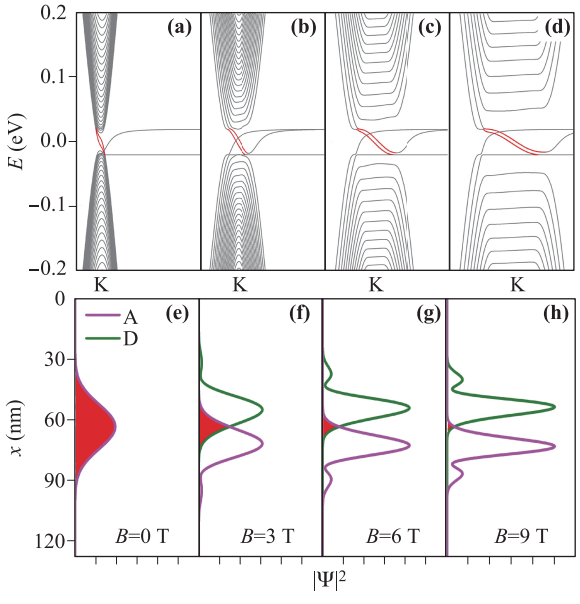

Fig. 2 Band structure of the BLG line junction with zigzag boundary at different magnetic fields $B = 0$ **(a)**, 3 **(b)**, 6 **(c)**, and 9 T **(d)**. The device length is $d = 127.8$ nm, the junction width is $w = 85.2$ nm, and the layer potential difference is $2U = 40$ meV. The formation of the Landau levels lifts the bound states away from the energy range of the kink states (red). **(e–h)** Corresponding wavefunction distributions of the kink states in valleys K and K′ [modes A and D, respectively, labeled in Fig. 1 (b)], showing increasing separation as B increases.

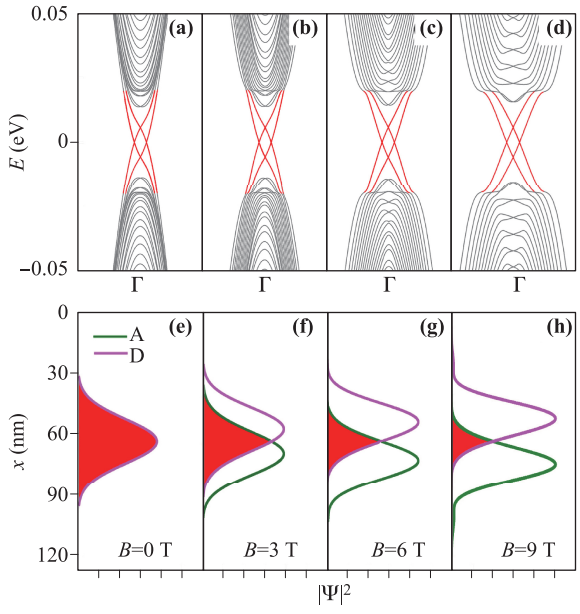

Fig. 3 Band structure of the BLG line junction with armchair boundary at different magnetic fields $B = 0$ **(a)**, 3 **(b)**, 6 **(c)**, and 9 T **(d)**. The sizes of device and on-site potential are the same as in Figs. 2. Corresponding wavefunction distributions of the kink states around Γ point [modes A and D, respectively, labeled in Fig. 1(c)], showing increasing separation as B increases.

Furthermore, in the presence of magnetic field, the wavefunction distribution can be tuned by varying the Fermi energy electrically, as shown in Figs. 4(a)–(d) and Figs. 5(a)–(d). In these figures, the magnetic field is set to 9 T. By increasing the Fermi energy from $E_F = 0$ eV to $E_F = 0.015$ eV, we find that the ZLM wavefunction in valley K (K′) moves upward (downward) and the ZLM wavefunction in Γ point also moves the same way. At the charge neutrality point of $E_f = 0$, the wavefunctions almost coincide with each other.

In brief, the presence of magnetic field not only separates the ZLMs and bulk states by a larger band gap but also spatially separates the counter-propagating ZLMs. Both effects can effectively suppress the backscattering of the ZLMs. Thus, the presence of magnetic field is expected to strongly enhance the robustness of the ZLMs.

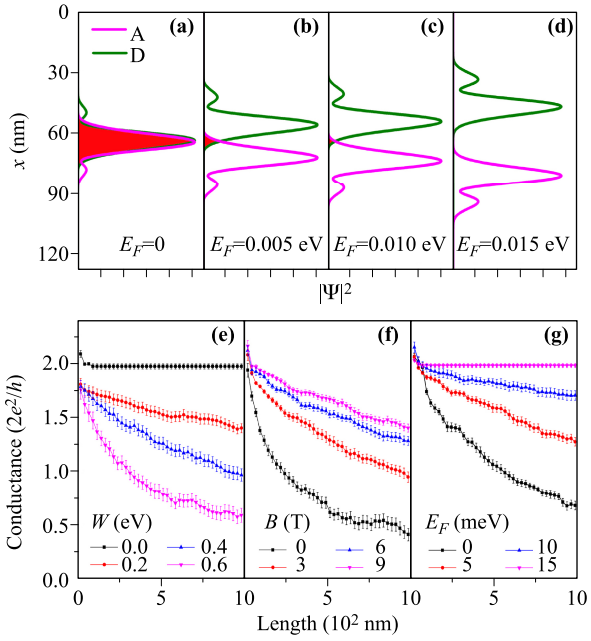

Fig. 4 **(a–d)** Corresponding wavefunction distributions of the kink states in valleys K and K′ (modes A and D, respectively, labeled in Fig. 1(c)) at different Fermi energies $E_F = 0$ **(a)**, 0.005 **(b)**, 0.010 **(c)**, and 0.015 eV **(d)** but the same magnetic field strength $B = 9$ T. **(e, f)** Average conductance vs. device length under different parameter strengths. In (e), the Fermi level is $E_F = 0.01$ eV, there is no magnetic field, and the disorder strength is varied as $W = 0$, 0.2, 0.4, and 0.6 eV. The band gap is set as $2U = 0.04$ eV. In (f), the Fermi level is $E_F = 0.006$ eV, the magnetic field strength is varied as $B = 0$, 3, 6, and 9 T, and the disorder strength is $W = 0.6$ eV. In **(g)**, the magnetic field strength is $B = 9$ T, the Fermi level is varied as $E_F = 0$, 5, 10, and 15 meV, and the disorder strength is $W = 0.06$ eV. Each point is an average of 30 samples with different disorder configurations.

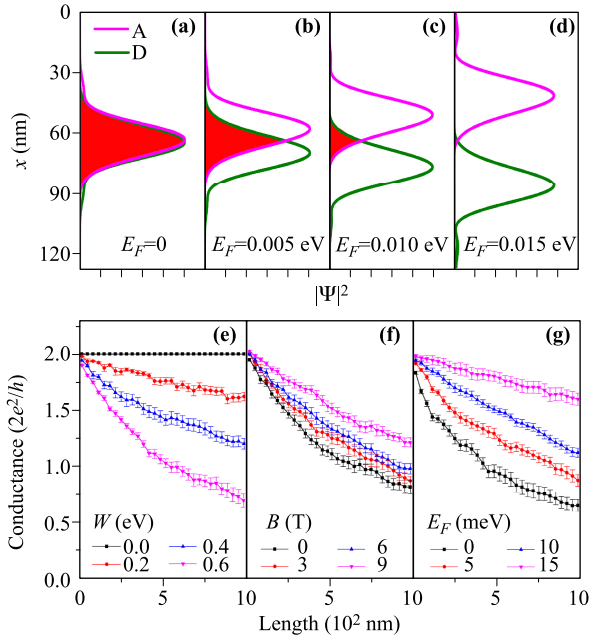

Fig. 5 **(a–d)** Corresponding wavefunction distributions of the kink states around Γ point (modes A and D, respectively, labeled in Fig. 1(c)) with the same parameters as in Figs. 4(a)–(d). **(e–g)** Average conductance vs. device length under the parameter strengths same as in Figs. 4(e)–(g).

To demonstrate the influence of the magnetic field, Fermi energy, and disorder, we also study the ZLM conductivity for junctions of different lengths. We begin by studying the case which is in the absence of a magnetic field, as shown in Fig. 4(e) and Fig. 5(e), where we find a quantized conductance that is independent of the junction length in the absence of a disorder. As the disorder strength is increased, the conductance decreases with an increase in the system length. For a disorder strength of $W = 0.6$ eV, the conductance decreases to a value of 1 e^2/h for a junction length of 1 μm. At the same disorder strength, the conductance is increased by applying magnetic field, as shown in Fig. 4(f) and Fig. 5(f). In the presence of a magnetic field of 9 T, the conductance of the 1 μm junction is increased by a factor of three for junction with zigzag boundary. But for junction with armchair boundary, the increase in conductance is not as strong as in zigzag boundary condition. This can be understood by comparing Figs. 2(e) and (f) and Figs. 3(e) and (f), the separation of corresponding wavefunction distributions of the kink states for zigzag boundary condition is larger than that for armchair boundary condition under the same magnetic field strength. The enhancement of the conductivity by the magnetic field becomes increasingly obvious as the Fermi energy deviates from the charge neutrality point, as shown in Fig. 4(g) and Fig. 5(g), under a magnetic field of 9 T. In this figure, we find that at the charge neutrality point of $E_F = 0$, even under magnetic field of 9 T, the conductance decreases to approximately 1 e^2/h. As the Fermi energy is gradually increased for both boundary condition, the influence of the disorder on the conductivity becomes weaker. For zigzag boundary condition, a quantized conductance of a sample as long as 1 μm can be realized when the Fermi energy reaches 0.015 eV; for armchair boundary condition reaching the same Fermi energy, the conductance of the 1 μm junction is increased by a factor of three.

Nevertheless, the influence of the magnetic field becomes reduces as the band gap increases. In Figs. 6(a)–(d) and Figs. 7(a)–(d), we plot the band structure for differing layer potential difference U with the same magnetic field strength and Fermi level. We find that the band gap increases with the layer potential difference. The ZLM wavefunctions are also shown in Figs. 6(e)–(h) and Figs. 7(e)–(h). We find that the spatial separation becomes considerably increases with decrease of the band gap for both boundary condition. This is because increasing the layer potential difference enhances the electron confinement, and the wavefunctions are restricted to the

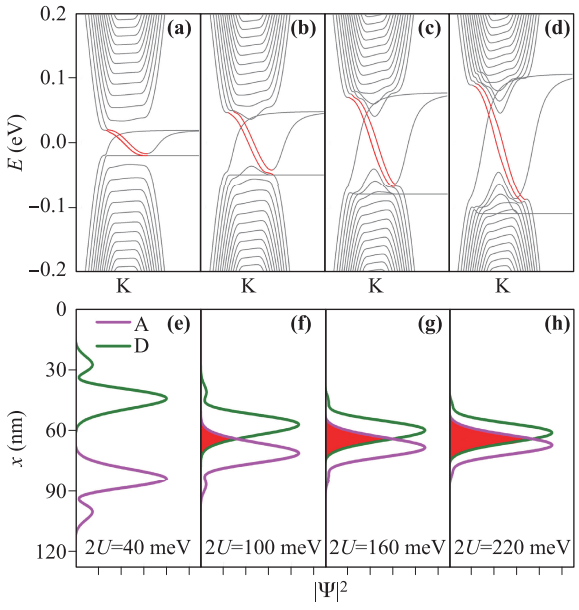

Fig. 6 **(a–d)** Band structures of the BLG line junction with zigzag boundary calculated with $2U = 40$ **(a)**, 100 **(b)**, 160 **(c)**, and 220 meV **(d)**, a magnetic field strength of $B = 6$ T, and a Fermi level of $E_F = 12$ meV. Increasing U increases the energy range in which only the kink states (marked in red) exist. **(e–h)** Corresponding wavefunction distributions of the kink states in valleys K and K′ [modes A and D, respectively, labeled in Fig. 1(c)], showing increasing separation as the layer potential difference U is decreased.

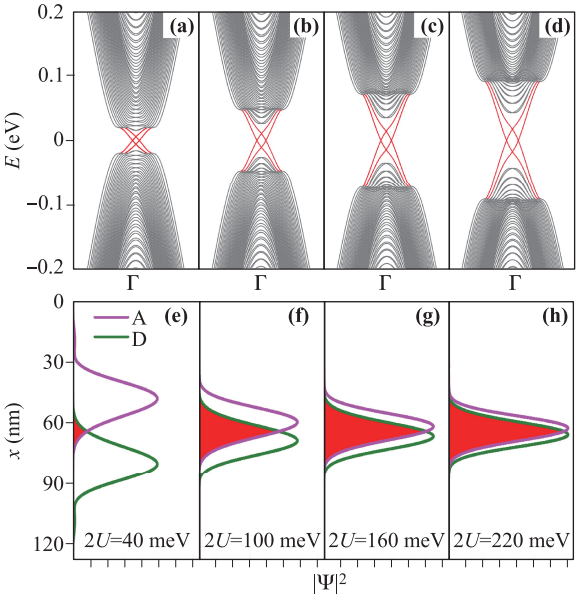

Fig. 7 **(a–d)** Band structures of the BLG line junction with armchair boundary calculated with the same parameter as in Fig. 6. Increasing U increases the energy range in which only the kink states (marked in red) exist. **(e–h)** Corresponding wavefunction distributions of the kink states around Γ point, showing increasing separation as the layer potential difference U is decreased.

interface between the left and right regions, meaning that there is no room for the wavefunctions to move.

In summary, we systematically studied the effect of magnetic field on the ZLM transport properties at different band gaps and Fermi energies, also for different boundary condition. We found that the presence of magnetic field not only enlarges the band gap, separating the ZLMs from the bulk states by a larger energy gap, but also spatially separates the wavefunction distributions of counter-propagating ZLMs. Furthermore, we found that decreasing the layer potential difference increases wavefunction separation. Both effects strongly enhance the robustness of ZLMs against a disorder. By calculating the ballistic length of the ZLMs under different disorder strengths, we numerically confirmed that the presence of magnetic field can effectively enlarge the ballistic length. Moreover, we found that the spatial separation of the counter-propagating ZLMs depends strongly on the Fermi energy. Under moderate magnetic field, increasing the Fermi energy from the charge neutrality point of $E_F = 0$ increases the distance between counter-propagating ZLMs. Such an effect makes the ZLM transport property highly tunable by magnetic field. These findings provide a new strategy for enhancing the robustness of ZLMs.

Acknowledgements This work was financially supported by the National Key Research and Development Program (Grant No. 2017YFB0405703), the China Government Youth 1000-Plan Talent Program, and the National Natural Science Foundation of China (Grant No. 11474265). We are grateful to the Supercomputing Center of USTC for providing high-performance computing assistance.

References

1. M. Bttiker, Edge-state physics without magnetic fields, *Science* 325(5938), 278 (2009)
2. G. W. Semenoff, V. Semenoff, and F. Zhou, Domain walls in gapped graphene, *Phys. Rev. Lett.* 101(8), 087204 (2008)
3. I. Martin, M. Blanter, and A. F. Morpurgo, Topological confinement in bilayer graphene, *Phys. Rev. Lett.* 100(3), 036804 (2008)
4. W. Yao, S. A. Yang, and Q. Niu, Edge states in graphene: From gapped flat-band to gapless chiral modes, *Phys. Rev. Lett.* 102(9), 096801 (2009)
5. M. Killi, S. Wu, and A. Paramekanti, Band structures of bilayer graphene superlattices, *Phys. Rev. Lett.* 107(8), 086801 (2011)
6. Y. Ran, Y. Zhang, and A. Vishwanath, One-dimensional topologically protected modes in topological insulators with lattice dislocations, *Nat. Phys.* 5(4), 298 (2009)
7. Y. B. Zhang, Y. W. Tan, H. L. Stormer, and P. Kim, Experimental observation of quantum Hall effect and Berry's phase in graphene, *Nature* 438, 201 (2005)

8. K. S. Novoselov, Z. Jiang, Y. Zhang, S. V. Morozov, H. L. Stormer, U. Zeitler, J. C. Maan, G. S. Boebinger, P. Kim, and A. K. Geim, Room-temperature quantum Hall effect in graphene, *Science* 315(5817), 1379 (2007)
9. C. Z. Chang, J. S. Zhang, X. Feng, J. Shen, Z. C. Zhang, M. H. Guo, K. Li, Y. B. Ou, P. Wei, L. L. Wang, Z. Q. Ji, Y. Feng, S. K. Ji, X. Chen, J. F. Jia, X. Dai, Z. Fang, S. C. Zhang, K. He, Y. Y. Wang, L. Lu, X. C. Ma, and Q. K. Xue, Experimental observation of the quantum anomalous Hall effect in a magnetic topological insulator, *Science* 340(6129), 167 (2013)
10. Z. Qiao, S. A. Yang, W. Feng, W. K. Tse, J. Ding, Y. Yao, J. Wang, and Q. Niu, Quantum anomalous Hall effect in graphene from Rashba and exchange effects, *Phys. Rev. B* 82(16), 161414R (2010)
11. L. Sheng, D. N. Sheng, and C. S. Ting, Spin-Hall effect in two-dimensional electron systems with Rashba spin-orbit coupling and disorder, *Phys. Rev. Lett.* 94(1), 016602 (2005)
12. Z. H. Qiao, J. Jung, Q. Niu, and A. H. MacDonald, Electronic highways in bilayer graphene, *Nano Lett.* 11(8), 3453 (2011)
13. T. Hou, G. H. Chen, W.K. Tse, C. G. Zeng, and Z. H. Qiao, Topological zero-line modes in folded bilayer graphene, arXiv: 1809.04036 (2018)
14. K. Wang, Y. F. Ren, X. Z. Deng, S. A. Yang, J. Jung, and Z. H. Qiao, Gate-tunable current partition in graphene-based topological zero lines, *Phys. Rev. B* 95(24), 245420 (2017)
15. Z. H. Qiao, J. Jung, C. Lin, Y. F. Ren, A. H. MacDonald, and Q. Niu, Current partition at topological channel intersections, *Phys. Rev. Lett.* 112(20), 206601 (2014)
16. J. Li, K. Wang, K. J. McFaul, Z. Zern, Y. F. Ren, K. Watanabe, T. Taniguchi, Z. H. Qiao, and J. Zhu, Gate-controlled topological conducting channels in bilayer graphene, *Nat. Nanotechnol.* 11, 1060 (2016)
17. M. Kim, J. H. Choi, S. H. Lee, K. Watanabe, T. Taniguchi, S. H. Jhi, and H. J. Lee, Valley-symmetry-preserved transport in ballistic graphene with gate-defined carrier guiding, *Nat. Phys.* 12(11), 1022 (2016)
18. L. Ju, Z. Shi, N. Nair, Y. Lv, C. Jin, H. A. Velasco, M. C. Bechtel, A. Martin, J. Zettl, Analytis, and F. Wang, Topological valley transport at bilayer graphene domain walls, *Nature* 520(7549), 650 (2015)
19. S. Datta, Electronic Transport in Mesoscopic Systems, Cambridge University Press, 1997
20. M. P. L. Sancho, J. M. L. Sancho, and J. Rubio, Quick iterative scheme for the calculation of transfer matrices: Application to Mo(100), *J. Phys. F Met. Phys.* 14(5), 1205 (1984)